**Open Access**

**Research Article**

# Spatiotemporal Thermal Contours mapping of *ex-vivo* Bovine Liver Radiofrequency Thermal Ablation utilizing Hyperspectral Image and its Associated K-Mean Clustering Algorithm

**Mohamed Hisham Aref,**[a*] **Ibrahim H. Aboughaleb,**[a] **Mohamed Rabie,** [a] **Yasser H. El-Sharkawy**[a]

[a]Military Technical College, Biomedical Engineering Department, El-Fangary Street, Cairo, EGYPT

**\*Corresponding author:** Mohamed Hisham Aref, Military Technical College, Biomedical Engineering Department, El-Fangary Street, Cairo, EGYPT. E-mail: Mh-aref@ieee.org

**Abstract:**

**Significance:** Hepatocellular carcinoma (HCC) is considered as worldwide health problem with a poor diagnosis due to limited detection techniques. Thermal ablation is the dominant modality to treat liver tumors for discriminating patients who are not allowed to have surgical intervention. Knowing that, observing or foreseeing the size of the subsequent tissue putrefaction during the Thermal Ablation techniques is a difficult undertaking.

**Aim:** To examine the impacts of ablation zone volume following Radiofrequency ablation (RFA) of an ex-vivo bovine liver to correlate the impacts of thermal ablation with target organ perfusion; by exploiting the unique properties of Hyperspectral Imaging (HSI).where, Vessels may source cooling in the adjacent tumor target (heat-sink-effect) with risk of cancer recurrence and the infiltration profundity estimations consider the lessening of the tissue.

**Materials and Methods:** Radiofrequency ablation was perfused on ex-vivo bovine livers at peripheral and central-vessel-adjacent locations, and monitored by HSI with a spectral range from 400 to 1000 nm. The system contains k-means clustering (K=8) algorithms combining spectral and spatial information. Labeled spectral signatures datasets were used as training data. Statistical analysis (10 samples) was computed to calculate the highest variance between six spectral images for determining the optimum wavelength for discrimination between the affected regions after thermal ablation (normal, thermal, and ablated liver tissue regions).

**Results:** The change of the optical properties of ex-vivo liver tissues provides different responses to light transmission, scattering, absorption and particularly the reflection over the spectrum range. The spectral reflectance signatures were measured and evaluated using designed K-mean clustering algorithm after image reconstructed. Trials showed that spectral region 650~650 nm was proposed as optimum spectral range. Where, these results successfully distinguishes the Surface Thermal ablation region (x,y-axis),as well as the Thermal penetration Depth (z-axis) for Tissue characterization and Contour mapping for the unwanted thermal damage.

**Conclusions:** Hyperspectral imaging is a powerful tool in real-time monitoring the thermal ablation and more accurate compared to the conventional imaging modality.

**Keywords:** Liver Tumor; Hyperspectral Imaging; RF Thermal Ablation; K-mean Clustering Algorithm, Tissue Thermal depth.

## 1. Introduction

Liver malignancy is the $5^{th}$ most common tumor and the $2^{nd}$ most prominent reason for tumor-related passing around the world, and more than (800,000) deaths are accounted for globally every year [1], [2]. In Egypt, there has been a noteworthy increment in the extent of hepatocellular carcinoma (HCC) among interminable liver disease patients [3]. Hepatocellular carcinoma (HCC) is the most well-known essential dangerous tumor in the liver, particularly in patients with cirrhosis[4]. Confirmed patients with HCC follow a specific system for stage classifier and best treatment opportunity, such as the Barcelona Clinic Liver Cancer (BCLC) stage system [5].

Liver successful transplantation is considered the best option for HCC treatment for eligible patients [2], [6], [7]. However, transplantation is constrained by the accessibility of liver contributors and by the available budget [8]. Another great restorative alternative for initial-phase HCC patients with the non-cirrhotic liver is hepatic resection[9]. Fractional hepatectomy gives shorter holding up times and practically identical 5-year endurance rates (60~70%) contrasted with transplantation [10].On the other hand, the number of colorectal metastases (CLM) patients qualified for resection is less than 20% because of incompatible tumor areas and worsened residual liver function [11].

Negligibly intrusive thermal ablation, including laser interstitial thermotherapy [12], radio-frequency Ablation (RFA) [13], microwave Ablation(MWA)[14], [15], and high-Intensity ultrasound (US) (interstitial [16], focused [17], and unfocused [18]) ablation. All these modalities is a significant treatment way to deal with unresectable essential and secondary liver tumors (e.g., HCC and CLM) [13], [18], [19].

Thermal ablation may likewise be utilized to help careful resection to diminish intraoperative blood loss and postoperative hospitalization [13]. While it is considered being the most fitting alternative track for HCC long-suffering patients who are unqualified for both transplantation and resection. This track is usually used for the patients who have tumor size ≤ 3 cm, in light of the Barcelona Clinic Liver Cancer (BCLC) classification framework [5], [13].

Even-though, RF ablation is more affordable, less obtrusive, and with lower difficulty rates than incomplete resection in early hepatocellular carcinoma (HCC) and small colorectal metastases [20], [21]. However, it is not the ideal modality due to the inability to monitor the thermal effect with the conventional image-guided techniques, such as the Computed Tomography (CT) and ultrasound due to the struggle of separation of feasible and destructed tissue and distinguishing proof of the tumor edges, as a result of tissue scarring and gas bubble fact which emerge during the thermal procedure [22],[23], [24].

Imaging modalities are vital for real-time observing of thermal tissue variations throughout laser interstitial thermotherapy, RFA, MWA, HIFU, or bulk thermal ablation [25], [26]. MRg-HIFU has been utilized for observing and control of thermal removal utilizing real-time MR thermometry[27], [28]. Knowing that MRg-HIFU escalations treatment therapy is expensive and difficult [29], [30]. USg-HIFU is more convenient and low-cost, while its high edge rate, constant ability conceivably makes it increasingly equipped for ablating versatile organs[31], [32].

Recently, many researchers have developed several imaging methods to guarantee suitable removal of liver malignant and metastases utilizing non-intrusive or negligibly obtrusive systems with respect to the conventional excisional biopsy. Of these imaging techniques, infrared thermography monitoring [33], [34],contrast-enhanced ultrasound [35], real-time ultrasound elastography ,high resolution US [36], [37] and electrode vibration elastography[38].This exploratory investigation was the leading at the attainability of HSI observing in RFA .On the other side hyperspectral imaging (HSI) method provides a specific wavelengths (spectral image) across the electromagnetic spectrum as it collects spatial and spectral information for the specimen under investigation [39], [40].

Spectral imaging is otherwise called imaging spectroscopy, which introduces the innovation that incorporates conventional imaging and spectroscopy techniques to acquire both spatial and spectral data of an object [41]. It was at first described in the late 1980s for remote distinguishing of the Earth [42]. Spectral imaging can be separated into multispectral imaging, hyperspectral imaging (HSI), as per its unearthly goals, the number of groups, width, and continuity of groups[43], [44]. Multispectral imaging frameworks, for the most part, gather information in few and generally noncontiguous wide ghastly groups, regularly estimated in micrometers or several micrometers. These ghastly groups are chosen to gather power in explicitly characterized pieces of the range

and advanced for specific classes of data generally clear in those groups. While HSI frameworks can gather many object groups [40], [41].

HSI is a rising imaging methodology, and promising outcomes have been appeared as for malignant growth identification in the brain. Where, two HS camera is used covering the spectral range of 400–1700 nm, the system is able in ~1 min to discriminate between normal and malignant tissue in the brain tissue thru neurosurgical procedures [45]. Study on gastric tumors in 10 human subjects. Where, the spectral monograms were obtained and evaluated in normal and Tumor tissue. Processing methods with the standard deviation of the spectral graph, support vector machine, and the 1st derivatives were recommended to improve and detect the Tumor regions. The 1st derivatives in spectral region between 1226~1251 nm and 1288~1370 nm were suggested as criteria that successfully discriminate between normal and Tumor tissue[46].

Moreover, in the HSI in medical applications, ultrasonic thermos-elastic emissions were produced in breast tissue by the inclusion of nanosecond laser pulses at 1064 nm generated by a Q-switched Nd: YAG laser. Where the differences in photoacoustic reaction signatures of normal and malignant breast tissue were found to be highly enhanced[47]. In the prostate tumor, the HSI framework was utilized to catch in-vivo pictures of rats influenced by human prostate tumors. The results upon 11 mice proved that the sensitivity and specificity of the HSI classification technique are 92.8% to 2.0% and 96.9% to 1.3%, respectively [48].

This pilot study demonstrates the objective of building and implementation a custom optical imaging system and associated K-mean clustering algorithm using to characterized and evaluate different thermal effects of investigated ex-vivo bovine liver samples. This non-invasive system can provide virtual information for a medical doctor, helping in early perception during surgery by improving tissue visibility and an early admonition to maintain a strategic distance from tissue fibrosis and thermal impact utilizing electrosurgical generator or any other Surgery/Thermal ablation modality [47][49].

## 2. Materials and Methods

In this sector, exploratory arrangement and techniques for a progression of examinations on controlled thermal ablation of *ex-vivo* Bovine liver tissue are talked about. In these analyses, where all the pieces of the framework and their interconnections are exhibited in Figure 1. Seven different elements compose the system acquisition platform for tissue characterization (Hyperspectral camera / CCD microscopic camera / Thermal camera / RF generator / Light source / Computer & its Image processing software / Liver sample posed on the white optical board).

### 2.1 Sample preparation:

Experimental under test samples (Bovine Liver Tissue) A freshly cut out bovine liver was attained from a local abattoir in EGYPT and placed in ice-box with deionized saline, Liver tissue samples were cut with measurements (5 cm × 6 cm), Analysis were performed at room temperature 25 °C, with a normal liver temperature of 23°C~ 25°C estimated before every preliminary and stored in refrigerator up to –70°C.

### 2.2 Optical imaging system for liver sample ablation monitoring:

To capture the necessary images Hyperspectral (HS) Camera was utilized (Brand: Surface Optics –Model: SOC710) this model has spectral range (400 to 1000 nm), 5 nm spectral resolution, pushbroom (line-scanning) and 10 degrees field of view. The camera incorporated with a lens (Schneider KREUZNACH XENOPLAN 1.9/35 CCTV-LENS 400 bis 1000nm). For each sample, the spectral cube image composed of 128 frames, and each frame represented a spectrum image of a specific wavelength.

### 2.3 Thermal Ablation Set-up:

Radiofrequency Generator (RF) (Brand: Bowa, Model: ARC303) was used to generate the necessary heat in the liver tissue simulating equivalent case as the surgical theatre for liver cancer thermal ablation and have been continuously monitored the temperature by the Non-Contact thermal camera (Brand: FLIR, Model: ETS 320), where the ground plate have been cut and customized by the sample size and area under the liver tissue and the active electrode fixed with articulating arm with a specific inserting depth (2 cm) inside the tissue, where the sample dimension is (5×6 cm).

The experimental setup have been repeated by changing the RF Tip to measure initially the Surface Thermal (x,y axis) Tissue characterization as illustrated in Figure 1-a,as well as to Monitor the Thermal Depth (z axis) for Tissue characterization thermal penetration depth evaluation in the (Z-axis) as shown in Figure 1-b.
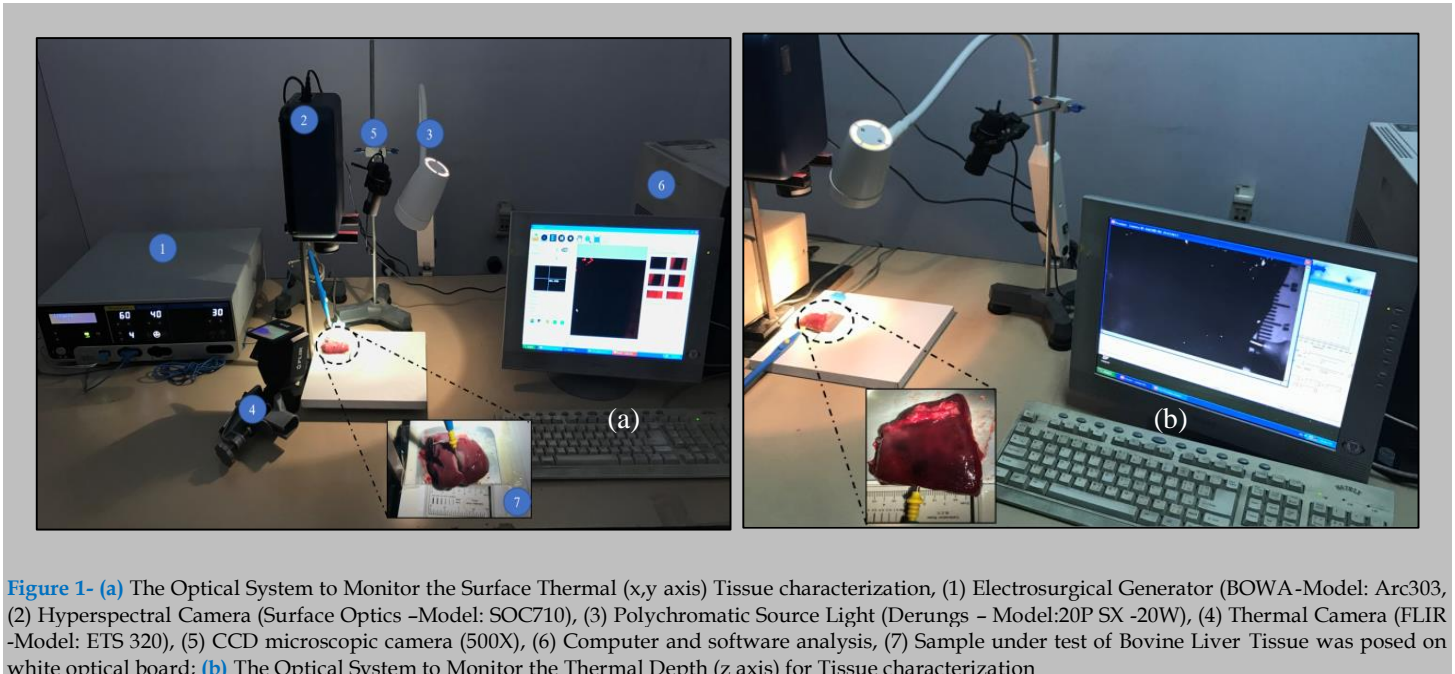


**Figure 1- (a)** The Optical System to Monitor the Surface Thermal (x,y axis) Tissue characterization, (1) Electrosurgical Generator (BOWA-Model: Arc303, (2) Hyperspectral Camera (Surface Optics –Model: SOC710), (3) Polychromatic Source Light (Derungs – Model:20P SX -20W), (4) Thermal Camera (FLIR -Model: ETS 320), (5) CCD microscopic camera (500X), (6) Computer and software analysis, (7) Sample under test of Bovine Liver Tissue was posed on white optical board; **(b)** The Optical System to Monitor the Thermal Depth (z axis) for Tissue characterization

### 2.4 Illumination System:

HS cameras require solid and exact brightening of the scene to be caught so as to stay away from outside obstructions created by the ecological light where the catch is being performed. The enlightenment framework utilized right now dependent on a polychromatic light (Brand: Derungs – Model: 20P SX -20 Watt) this model has spectral range (348 to 820 nm). This sort of light is reasonable for HS applications because of the high homogeneity of its range over the whole spectral range.

### 2.5 Experiment set-up:

Several experiments were repeated and implemented to reach the desired results needed to execute the necessary image analysis and signal processing upon the various sources of captured images. Revealed the RGB images with the CCD microscopic camera (500X) to monitor and record the thermal ablation process, additionally the thermal images by thermal camera (FLIR -Model: ETS 320) for monitoring the elevation of the thermal effect in the sample tissue during the ablation, supplementary to be used in image verification with our algorithm.

### 2.6 Monitoring Set-up:

HSI sensors produce a three-dimensional (3D) information structure, called HS block, where the spatial data is contained in the initial two measurements, while the third measurement incorporates the spectral data

[50], [51]. In a hyperspectral picture, every pixel has an arrangement of reflectance in various spectral frequencies that can show the spectral outline of that pixel [45]. On one hand, every pixel of the HS picture contains a full otherworldly mark of length equivalent to the quantity of spectral groups of the HS cube. On the other hand, a dark scale picture of the caught scene can be gotten utilizing any of the unearthly groups that shows the spatial data gave by the picture sensor at a specific frequency[52][50].

### 2.7 Hyperspectral picture conquering:

Six individual arrangements of hyperspectral pictures were gotten for each liver sample, each arrangement consisting of a (5 cm × 6 cm) of the liver sample arrangement on a lined tray. Line-scan images were captured for exposure times of 6 msec at 3.12 nm intervals, and each set consisted of 600 line scans corresponding to 600 × 502 pixels per spectral band. The hyperspectral images were composed of a total of 128 spectral bands in the range from approximate 379 to 1050 nm, incorporated with a lens with range (400 to 100 nm).

The drove light enlightens the liver tissue region of interest (ROI) and the camera target focal point gathers the radiation from the tissue and shows a picture on the passage way cut plane. The cut decides the field of imaging in spatial ways. The radiation from the cut is anticipated to the prism-grating; along these lines the bearing of engendering of the radiation changes on its wavelength. Each purpose of the tissue is

represented on the lattice detector by an arrangement of monochromatic focuses that makes a consistent range toward the unearthly hub.

### 2.8 Records standardization:

The issue with the spectral non-consistency of the light system and the impact of the dim current are wiped out through standardization of the picture information to discover the standardized reflectance of the sample. A standard reference white board was set in the area of imaging and its information were used as the white reference[44], [51].This white reference is a standard reflectance that ought to be utilized for information standardization which shows most extreme standard reflectance in every frequency and in catching time temperature. The reflectance from the board gives a gauge of the occurrence light on the organs at every frequency and standardizes the temperature changes, which is utilized in standardization of the range. The dull current was caught by keeping the camera shade shut. At that point the information was standardized to locate a relative reflectance, as clarified in equation (1):

$$RF(\lambda) = \frac{Rcrude(\lambda) - Rblack(\lambda)}{Rwhite(\lambda) - Rblack(\lambda)} \qquad (1)$$

Where $RF(\lambda)$ the determined relative reflectance esteem is for every Wavelength,$Rcrude(\lambda)$ is crude information brilliance estimation of a given pixel,$Rblack(\lambda)$ and $Rwhite(\lambda)$ are, correspondingly, the dull current and the white board brilliance obtained for each line and otherworldly band of the sensor.

### 2.9 Spectral mapping and Acquisition:

The captured HSI cube is analyzed upon the 128 frames regarding the spectral range to select the optimum contrast wavelength, after The selective image at wavelength 900 nm have been normalized, then applying moving average filter with kernel value =10, afterward K-mean clustering up to 8-clusters for the contour display of the ablation and thermal regions and color mapping to the sample tissue, finally overlay of the images to produce the final algorithm for the thermal detection to the sample.

Conversion of the hyperspectral image to the RGB image segmentation by normalization of the value of R, G and B in the range of [0, 1],as more explained with its conditions in equations (2-7), lastly these values is multiplied by 255 (8-bit conversion)[53].

$$n = \frac{N \times \pi}{180} \qquad (2); M = \frac{m}{100} \qquad (3); i = \frac{I}{255} \qquad (4)$$

$$x = i \times (1 - m) \qquad (5); y = i \times \left[ 1 + \frac{s \times \cos(n)}{\cos(\frac{\pi}{3} - n)} \right] \qquad (6)$$

$$z = 3i - (x + y) \qquad (7)$$

$$\text{If } n \le \frac{2\pi}{3} \text{ then } R = y; G = z \text{ and } B = x$$

$$\text{If } \frac{2\pi}{3} \le n < \frac{4\pi}{3} \text{ then } n = n - \frac{2\pi}{3}; R = x; G = y \text{ and } B = z$$

Then, applying the moving average filter, likewise well-known as arithmetic mean filter at kernel value 10 for noise removal and image enhancement [54].

$$f(x, y) = \frac{1}{hn} + \sum_{(k,L) \in W}^{\infty} \varphi(k, L) \qquad (8)$$

Where 'φ' is the noisy image, $f(x, y)$ is the restored image, and 'k' and 'L' are the row and column coordinates respectively, within a window 'W' of size 'h×n' where the operation takes place.

Next, applying the K-mean clustering (KMC) up to 8-clusters with variable threshold value from 0.2 up to 0.9 for variable thermal display, k-means is one of the least difficult unsupervised learning algorithms that take care of the clustering problem. We can formulate a general equation for the clustering algorithm; we can define the center-based clustering. Where variables define as $N = \{n_i \dots n_j\}$ is the set of (ń) data points to be

clustered in the d-dimensional, $S = \{s_i \dots s_j\}$ is the set of (Ќ) center points in the d-dimensional. The membership function $M(s_j|n_i)$ describes the proportion of the data set $n_i$ that related to the centroid $s_j$ with limitation $M(s_j|n_i) \ge 0$ and $\sum_j^K M(s_j|n_i) = 1$.A weight function $\hat{w} = (n_i)$ demonstrated how much effects data set $(n_i)$ in recalculation the new center with limitation $\hat{w} = (n_i) \ge 0$.

We can define the general model for the center-based clustering steps, as follows:

1.         Start the algorithm with deduced centers $(S)$.

2.         For each number point $(n_i)$,compute its membership $M(s_j|n_i)$ in each center $(s_j)$ and its weight $\hat{w} = (n_i)$.

3.         For each center $(s_j)$, recalculate its position from all data points $(n_i)$ according to their membership and weight.

$$s_j = \frac{\sum_{i=1}^{ń} M(s_j|n_i)\hat{w}=(n_i)n_i}{\sum_{i=1}^{ń} M(s_j|n_i)\hat{w}=(n_i)} \qquad (9)$$

4.         Repeat step#2 and step#3 until merging.

K-mean clustering (KMC) algorithm improves is:

$$KMC(N, S) = \sum_{i=1}^{n} \min_{j \in \{1 \dots K\}} \|n_i - s_j\|^2 \qquad (10)$$

This demonstrable function in equation (10) provides an algorithm which reduces the within-cluster variance.

$$(x + a)^n = \sum_{k=0}^{n} \binom{n}{k} x^k a^{n-k} \qquad (11)$$

The weight and membership functions concerning $KMC$ are:

$$M(s_j|n_i) = \begin{cases} 1 \text{ ; if } x = \arg min_j \|n_i - s_j\|^2 \\ 0 \text{ ; } otherwise \end{cases} \qquad (12)$$

$$w_{KMC}(n_i) = 1 \qquad (13)$$

Regarding the hyperspectral image justifications, each point in the liver tissue has a succession of relative reflectance in various wavelengths that makes the spectrum outline or unearthly mark of a point. The reflectance spectra of the pixels made out of thermal and ablated zones of a liver tissue surface were separated and used to compute a normal reflectance range. The degree of the thermal effect was divided into three levels (ablated, thermal influenced, and typical tissues), where these spectrum outlines have been assessed to discover a distinction between them in the tissue.

## 3. Results

Capturing the images with the Hyperspectral camera and processing the image before and after thermal ablation. Image normalization, moving average filter and K-mean clustering were utilized as channels to upgrade the thermal and ablated district in images caught with the hyperspectral camera. The capturing time for each image is about 5 ~ 12 sec and calculation time is < 20-sec using DADiSP/SE software (DSP Development Corporation,6.7 NI student edition B02, 2017) on a computer with processor Intel core i7 @1.8GHz with a 16 GB RAM. A conventional philosophy for target the identification and execution assessment was applied. The edges were balanced so as to expand the ablated recognition to guarantee identification of all the thermal /ablated districts. The exhibition was assessed utilizing the nature of discovery regarding the pathology.

After ablation, each sample was captured with the Hyperspectral camera, CCD microscopic camera (500X), and the thermal camera respectively thru several positions and at the same time for data recording purposes. Next, the liver sample was scanned at 1200 dpi to produce a high-resolution image to be used in image processing. Consequently, splitting it from the point of thermal ablation to explore more overall information about ablation and affected lateral cells to compare it with the captured

Hyperspectral data. Thermal ablation continuously captured by a thermal camera for temperature monitoring, as shown in Figure 2.
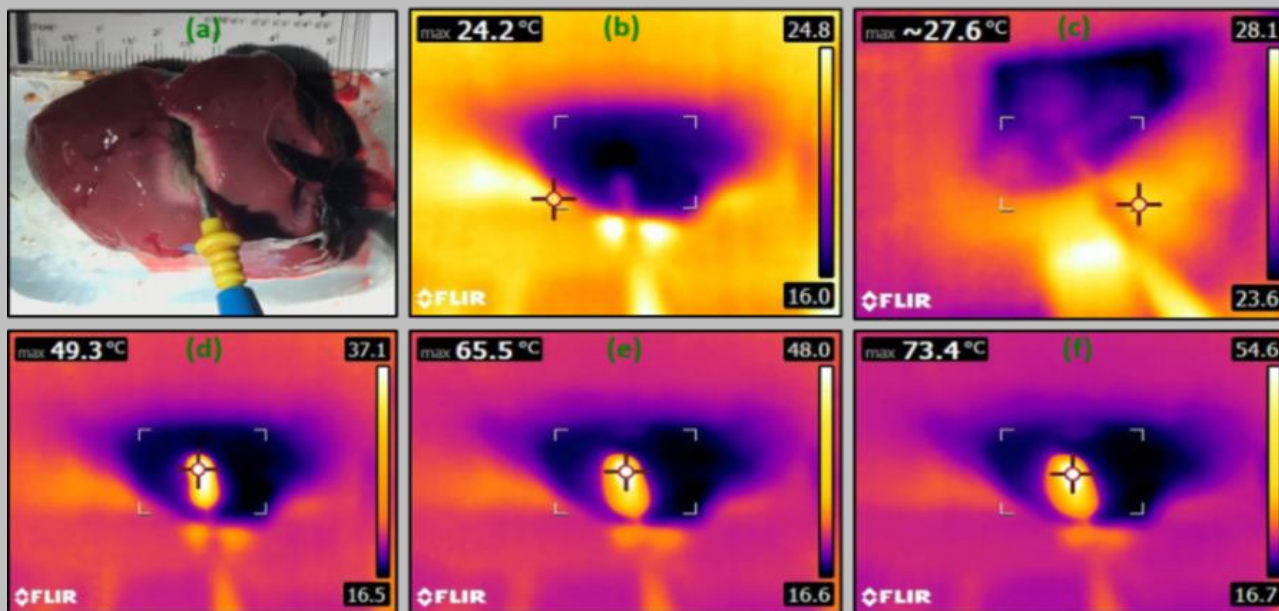


**Figure 2 -** The RGB image for liver tissue during thermal ablation captured by CCD camera; (a) Thermal image before ablation captured by thermal camera;(b) Thermal image after 2 Sec ablation at 27.6°C captured by thermal camera; (c) Thermal image after 3 Sec ablation at 49.3°C captured by thermal camera; (d) Thermal image after 4 Sec ablation at 49.3°C captured by thermal camera; (e) Thermal image after 5 Sec ablation at 65.5°C captured by thermal camera ; (f) Thermal image after 6 Sec ablation at 73.4°C captured by thermal camera.

The captured image of the ablation zone in *ex vivo* bovine tissue have been scanned at 1200 dpi for high image resolution shown in Figure 3 to compare it with the contour mapping analysis of the system algorithm to differentiate the unwanted thermal damage that was produced by heat conduction from the ablation tool, where heat conduction from the hot ablation zone along the ablation tool shaft have been more clearly appeared in the cross section View for the liver tissue and the penetration depth is shown by ablation tool tip which is approximately 2 cm long. Right and left piece for the bottom and top piece respectively in Figure 3-e.
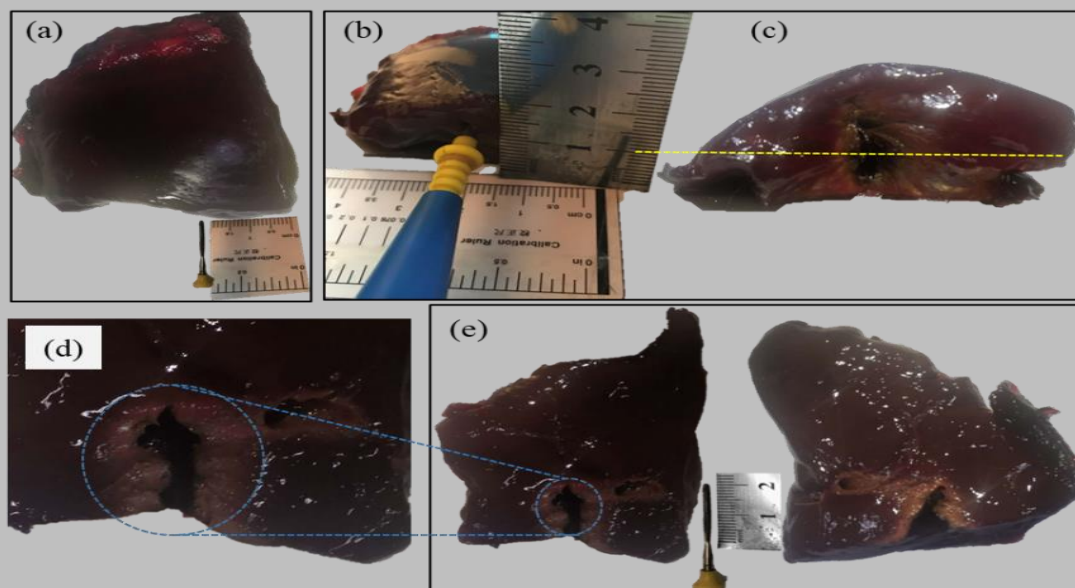


**Figure 3 -** Liver sample for Monitoring and evaluating the Thermal Depth (z-axis) for Tissue characterization; (a) Captured RGB image with CCD camera for Liver Tissue Sample before ablation; (b) Side View for Liver Sample after Thermal Ablation with specific location for RF Tip; (c) Side View for Liver Tissue Sample after Thermal Ablation without the RF Tip for more data clarification; (d),(e) Plan View of the Scanned Liver sample image (1200 dpi) Cross-Section View for liver tissue which maps the unwanted thermal damage that was produced by heat conduction from the ablation tool, heat conduction from the hot ablation zone along the ablation tool shaft.

The imaging method utilized with this camera is a pushbroom scanner; the cut passageway restricts the imaging field. By moving the camera between consequent pictures, inevitably all locales and wavelengths of the item are caught [52]. By reproducing the resulting pictures, a monochromatic unearthly picture for every wavelength can be developed, demonstrating the role of the wavelength to Spectacles or conceal specific information.

The deliberate optical spectra of biological tissues from 400 to 1000 nm spread the noticeable and can be separated at the atomic level, which extraordinarily adds to the reflectance esteems estimated in specific reaches. The test was performed utilizing the *ex-vivo* bovine liver tissue, where captured HSI is scanned and segmented, selecting specific points to measure the diffuse reflectance of the ablation region and two different positions around it for measuring the thermal effect with respect to the normal tissue, as illustrated in Figure 4-a.

These signals were drawn in the graph illustrating the unique spectral signatures of the normal, ablated and thermal regions, as demonstrated in Figure 4-b.the spectral reflectance between the normal signal (Green solid line) and the ablation region (Blue solid line) is more identified in wavelength ≥ 600 nm. However, to identify between the normal (Green solid line) and thermally affected tissue (Brown and Red solid line) it was more recognized in wavelength ≥ 500 nm.

we had used these spectral signatures as a guide for selecting the optimum spectral images which can be discriminate between the Four regions (Normal, Thermal#1, Thermal#2 and Ablation), to reduce the time of image processing for 128 frames to be only five spectral images starting from 500 nm up to 650 nm.
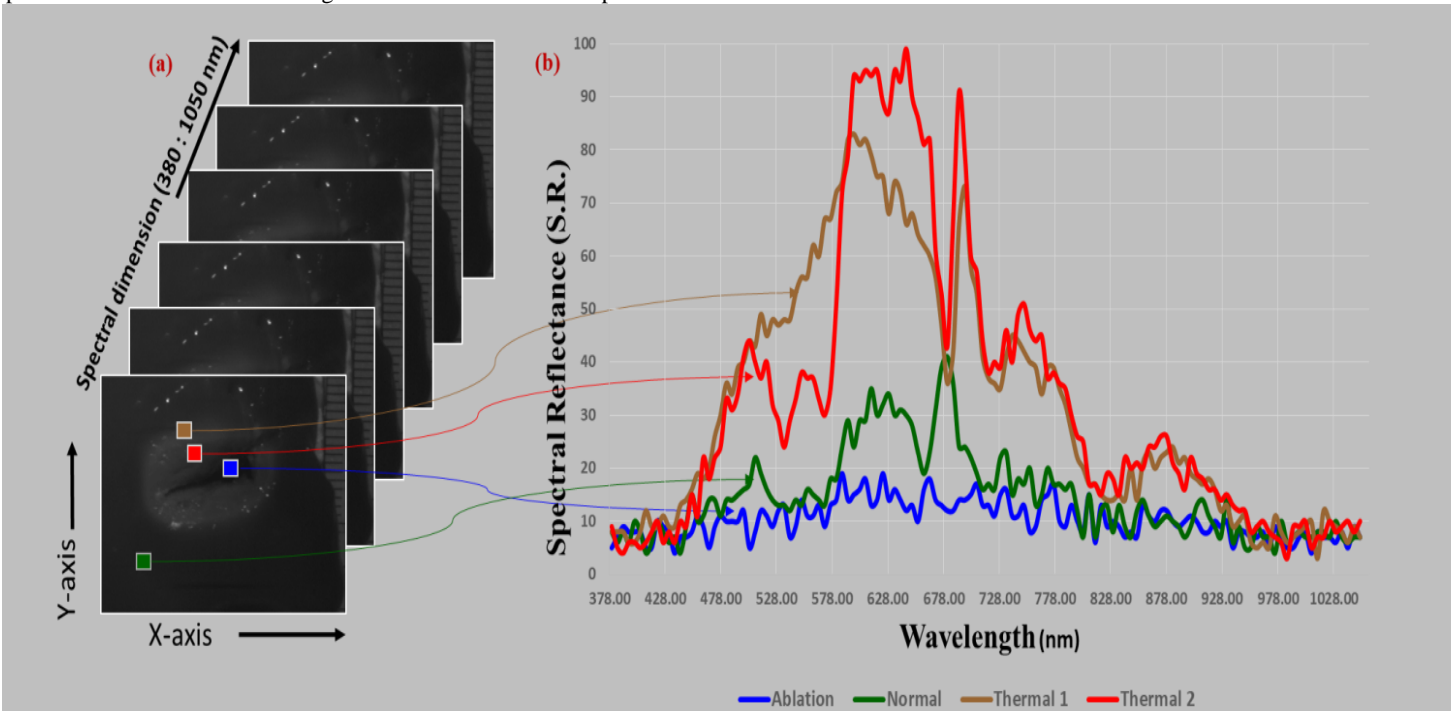


**Figure 4-** Hyperspectral image Signal Signature for pixel intensity of Liver Tissue ; (a) The Hyperspectral image segmentation captured in both the visible and Near IR range;(b) The blue pixel for demosntrate the reflectance of the Ablation region where its presented in the gragph by the blue solid line;the Green pixel is diffuse the reflectance of the Normal not affected with thermal region in the liver tissue where its presented in the gragph by the green solid line,additionaly the thermal#1 and thermal#2 regions is represented by red and brown pixel and solid lines repsectively.

The Captured spectral images of Bovine liver tissue after thermal ablation have been analysis and processed at various wavelengths to differentiate the pixel reflectance of the liver tissue. Spectral images within 400~800 nm addressed the discrimination between the ablated region, the normal region and the thermal effect degree on the liver tissue. The spectral image at wavelength range 600 ~ 650 nm is more distinguishable for the Thermal / Ablated zones, as previously clarified in Figure 4-b and more identified in the worksheet of Figure 5.

The various wavelengths in nanometers and the vertical hub of the demonstrating HSI segmentation where standardized reflectance of the liver tissue utilizing hyperspectral camera; the signal reflectance of the normal tissue is coded with (N) and plotted in Figure5-b; the signal reflectance of the Ablation Region is coded with (A) and plotted in Figure 5-c; the signal reflectance of Thermal #1 and Thermal#2 Regions is coded with (T1) and (T2) respectively plotted in Figure 5-c,e. According to the analysis of the signature signals in Figure 5-f which highlight that it's clearly identifying the thermal and ablated regions more at the wavelength region (600 ~ 650 nm).
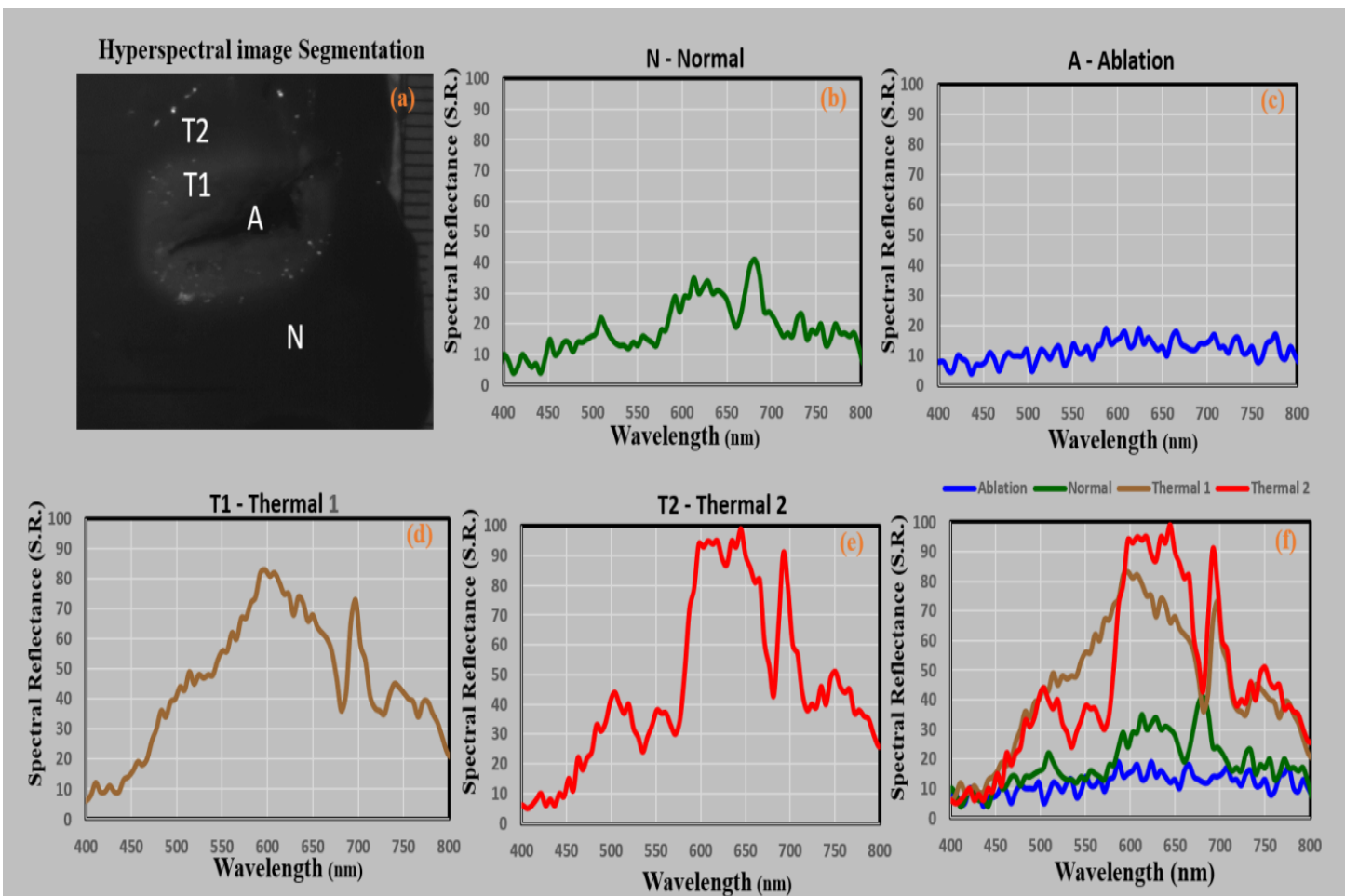
**Figure 5-** The flat pivot shows various wavelengths in nanometers and the vertical hub shows the standardized reflectance for the liver tissue by the hyperspectral camera; (a) Hyperspectral Image segmentation for the liver image by the hyperspectral camera after ablation ;(b) Illustrate the signal reflectance of the normal tissue; (c) Illustrate the signal reflectance of the Ablation Region; (d) Illustrate the signal reflectance of the Thermal#1 Region; (e) Illustrate the signal reflectance of the Thermal#2 Region (f) The complete reflectance signals of the selective regions (Thermal /Ablation / Normal).

The captured images of five spectral images starting from 500 nm up to 650 nm of the liver sample utilizing hyperspectral camera have been segmented for more image data, as shown in Figure 6-f. Then, applying normalization and Moving average filter (K=10) for noise removing.Finally, perform the Contour mapping with the K-mean image clustering (K=8) illuminating the thermal region and overlaying the contour mapping according to the threshold value over the original HSI to distinguish the selective surface thermal region in the liver sample for the surgeon, as illustrated in Figure 6-k and L respectively.

the experimental trails results that the Surface Thermal (x,y axis) Tissue characterization could be identified by the HS imaging with more details versus the visual inspection as illustrated in Figure 6,eventhough the thermal penetration depth evaluation in the (Z-axis) could not be visually identified but with the HS imaging it was clearly identified as shown in Figure 7.
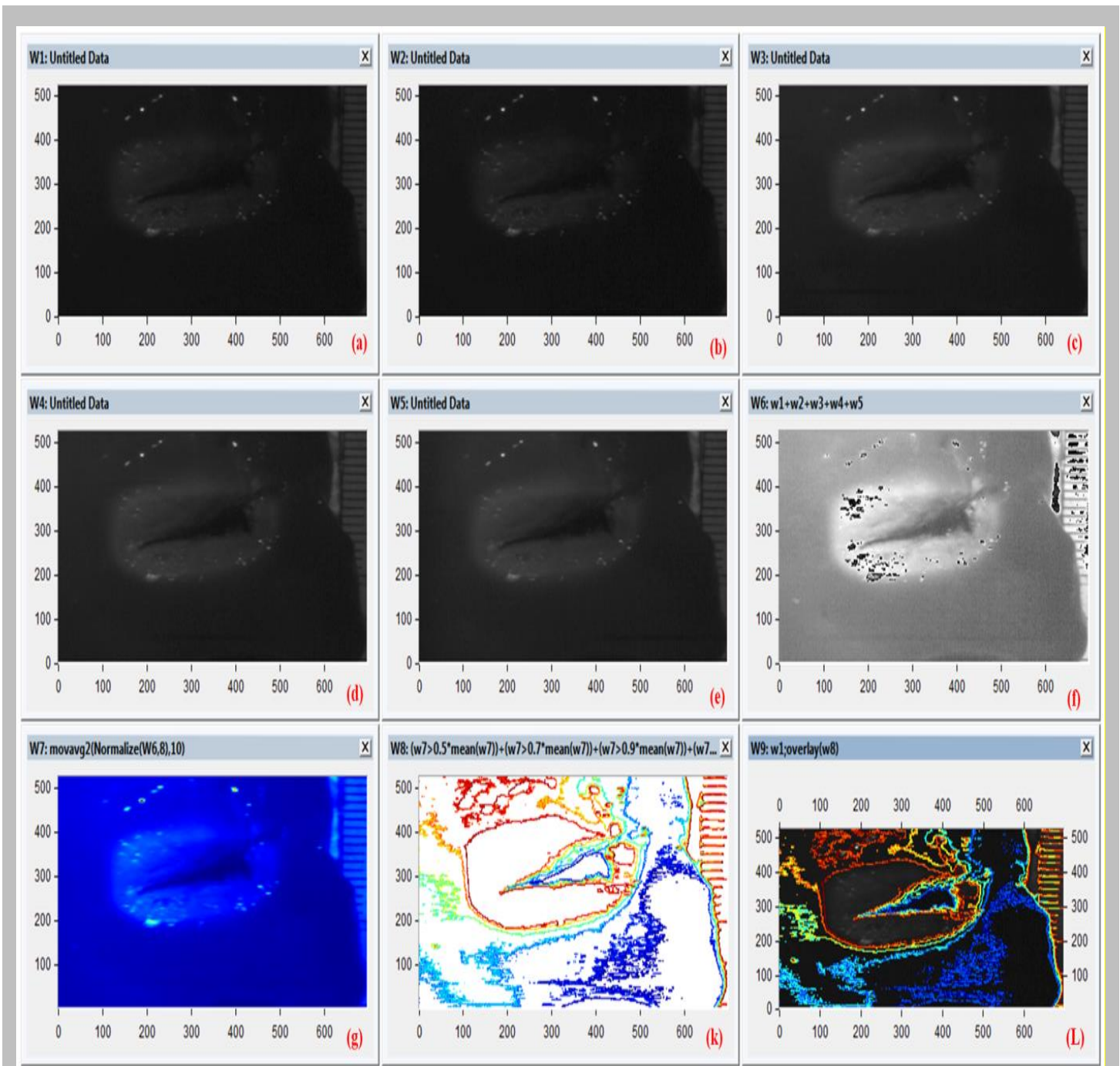
**Figure 6-** Image processing for captured HSI of liver sample at various wavelengths; (a) Spectral image at 500 nm ; (b) Spectral image at 550 nm; (c) Spectral image at 600 nm ;(d) Spectral image at 650 nm ; (e) Spectral image at 650 nm ; (f) HSI after segmentation for spectral range (500~650 nm); (g) HSI segmentation after normalization and Moving average filter (K=10) for noise removing ; (k) Contour mapping with the K-mean image clustering (K=8) at different threshold values for revealing the Thermal / Ablated effect region in the Liver sample ; (L) Overlaying the contour mapping over the original HSI.
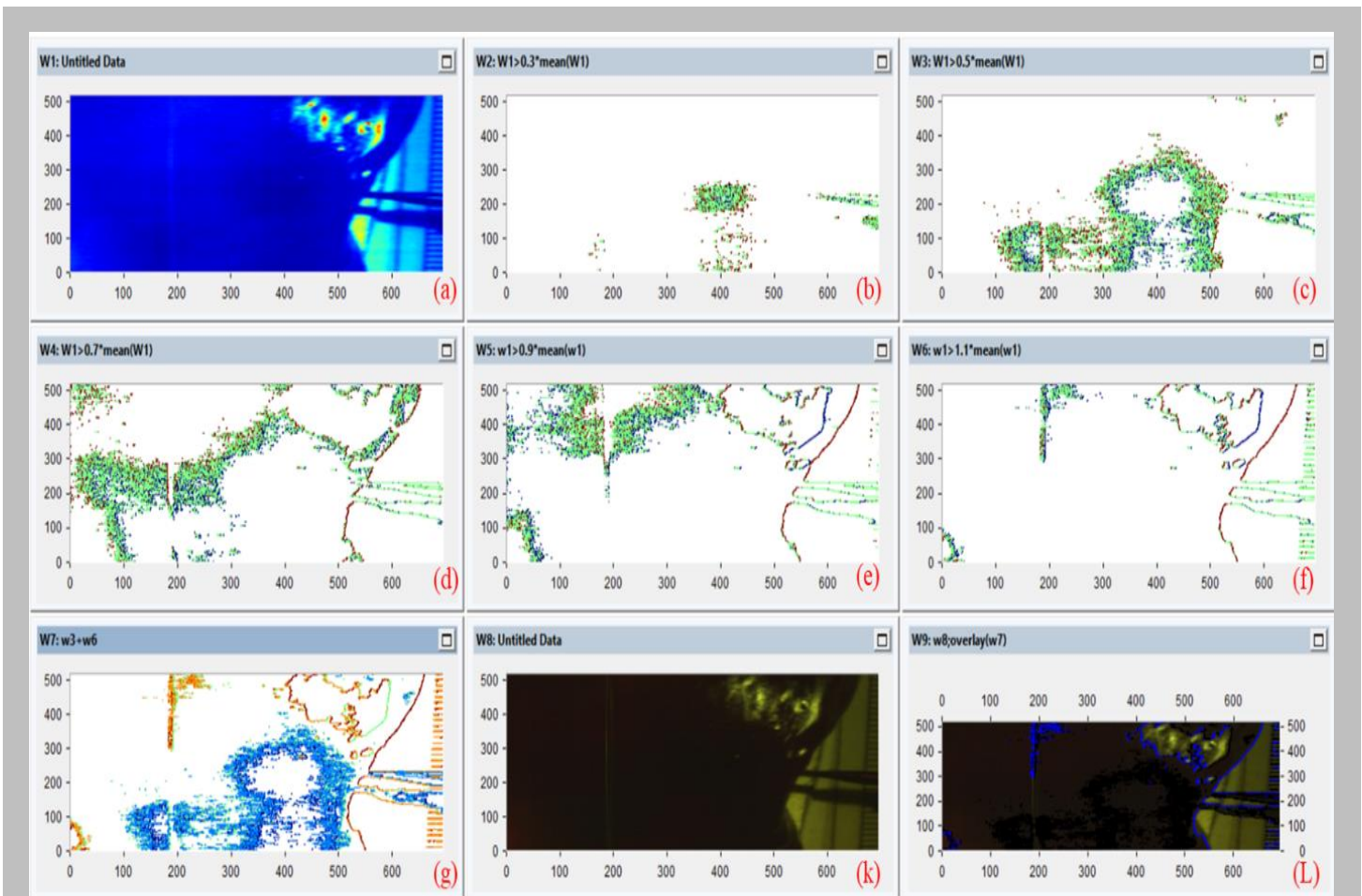
**Figure 7-** Image processing for captured HSI of liver sample segmentation for range (600~650 nm); (a) Image Normalization and Moving average filter (K=10) for noise removing; (b) Contour mapping with the K-mean image clustering (K=8) at threshold values (0.3) for revealing Normal regions in the Liver sample; (c) and (d) Contour mapping with the K-mean image clustering (K=8) at threshold values (0.5,0.7) for revealing Ablated regions in the Liver sample (e) and (f) Contour mapping at threshold value (0.9,1.1) for revealing Thermal region in the Liver sample; (g) Contour mapping for revealing Ablated /Thermal region in the Liver sample; (k) Hyperspectral RGB image segmentation for Liver sample; (L) Contour mapping for revealing higher Thermal region in the Liver sample.

## 4.  Discussion

Thermal ablation is the dominant modalities for ablative treatment of un-resection liver tumors, where monitoring the ablation process with the right image-guided inclusion of terminals is vital to accomplish a fruitful removal of tumors with minimum thermal damage of liver [34]–[37]. The removal procedure is routinely observed with computed tomography, or b-mode sonography to guarantee fruitful tumor removal with fitting wellbeing edges; however, tissue scarring or gas bubble development may hamper translation of sonographic pictures[20], [21], [33], [35].

Other imaging modalities like infrared thermography [33], [34], contrast-enhanced ultrasound [35], real-time ultrasound elastography, high-resolution US [36], [37], and electrode vibration elastography [38], which have been inspected to screen the ablation procedure. Anyway, all checking modalities have their issues to give an exact proclamation about the achievement of the ablation. On the other side hyperspectral imaging (HSI) method provides specific wavelengths (spectral image) across the electromagnetic spectrum as it collects spatial and spectral information for the specimen under investigation[39], [40].

Because of considerable between quiet spectral changeability which in

turn is reflected on the *ex-vivo* living tissue samples the developed algorithm encountered two main challenges: the high conditionality and the predetermined number of samples. Finally, the utilization of high spectral resolution HS cameras for thermal tissue examination permits analysts to concentrate in detail the optical properties of the tissues, distinguishing the most significant spectral diverts that are engaged with a specific application. The utilization of high spatial resolution HS cameras allows the examination of tests by joining the spectral and the morphological properties of the tissue, as illustrated in Figure 4 and Figure 5, respectively.

The work introduced in this paper with the objective of building up a custom optical imaging system and associated K-mean clustering algorithm to characterize and evaluate different thermal effects of the investigated *ex-vivo* beef liver sample before and after Radiofrequency ablation (RFA). The results demonstrated that the optimum wavelength range (600~650 nm) differentiated between the normal region, thermal, and ablated regions of the investigated samples.

However, Hyperspectral imaging is a powerful tool in monitoring the thermal ablation and more accurate compared to the conventional imaging modality, but it is very expensive regarding the commercial CCD camera

and it can`t work in real-time as the spectral cube need to be analyzed for the 128 frames and consume more time for image processing, and to avoid that topic we had to discriminate the optimum wavelength (600~650 nm), which decrease the time consuming and provide precise information to demonstrate significant monitoring of the ablation process to accomplish a fruitful ablation of tumors with minimum thermal damage of liver..

Our study was limited by *ex-vivo* liver tissue utilizing HS camera; further investigations will be carried out in the future work for validation using commercial CCD camera attached with the optical filter (720 nm) and several types of tissues with different properties.

## Declarations

The authors declare no conflict of interest and Stated that they have no competing interest. There are No funders and No one had any role in the design of the study; in the collection, analyses, or interpretation of data; in the writing of the manuscript, or in the decision to publish the results .This research did not receive any specific grant from funding agencies in the public, commercial, or not-for-profit sectors.

## Author Contributions:

- **Conceptualization:** Mohamed Hisham Aref, Ibrahim H. Aboughaleb, and Yasser H. El-Sharkawy**.**
- **Formal analysis:** Mohamed Hisham Aref, Ibrahim H. Aboughaleb, Mohamed Rabie
- **Investigation:** Mohamed Hisham Aref, Ibrahim H. Aboughaleb, Mohamed Rabie
- **Methodology:** Mohamed Hisham Aref, Ibrahim H. Aboughaleb, and Yasser H. El-Sharkawy
- **Resources:** Mohamed Hisham Aref, Ibrahim H. Aboughaleb
- **Image Algorithm:** Yasser H. El-Sharkawy
- **Supervision:** Yasser H. El-Sharkawy
- **Writing – original draft:** Mohamed Hisham Aref, Ibrahim H. Aboughaleb, Mohamed Rabie
- **Writing – review & editing:** Mohamed Hisham Aref, Ibrahim H. Aboughaleb, and Yasser H. El-Sharkawy

## References

[1] S. J. Yu, "A concise review of updated guidelines regarding the management of hepatocellular carcinoma around the world: 2010-2016," *Clin. Mol. Hepatol.*, vol. 22, no. 1, pp. 7–17, 2016, doi: 10.3350/cmh.2016.22.1.7.

[2] J. Ferlay *et al.*, "Cancer incidence and mortality worldwide: sources, methods and major patterns in GLOBOCAN 2012," *Int. J. cancer*, vol. 136, no. 5, pp. E359–E386, 2015.

[3] L. Mobarak, M. M. Nabeel, and W. El Agawy, "RISK FACTORS OF HEPATOCELLULAR CARCINOMA IN EGYPTIAN PATIENTS WITH CHRONIC LIVER DISEASE," *AL-AZHAR ASSIUT Med. J.*, vol. 13, no. 4, 2015.

[4] A. S. Ibrahim, H. M. Khaled, N. N. Mikhail, H. Baraka, and H. Kamel, "Cancer incidence in Egypt: Results of the national population-based cancer registry program," *J. Cancer Epidemiol.*, vol. 2014, 2014, doi: 10.1155/2014/437971.

[5] K. M. Kim, D. H. Sinn, S. Jung, G. Gwak, Y. Paik, and M. S. Choi, "The recommended treatment algorithms of the BCLC and HKLC staging systems : does following these always improve survival rates for HCC patients ?," no. September 2015, pp. 1490–1497, 2016, doi: 10.1111/liv.13107.

[6] T. Longerich, K. Breuhahn, and P. Schirmacher, *Molecular pathology of liver tumors*, vol. 9781461449. 2013.

[7] W. M. Rashed, M. A. M. Kandeil, M. O. Mahmoud, and S. Ezzat, "Hepatocellular Carcinoma (HCC) in Egypt: A comprehensive overview," *J. Egypt. Natl. Canc. Inst.*, vol. 32, no. 1, pp. 1–11, 2020.

[8] M. J. Englesbe *et al.*, "Sarcopenia and mortality after liver transplantation," *J. Am. Coll. Surg.*, vol. 211, no. 2, pp. 271–278, 2010.

[9] A. Forner, M. Gilabert, J. Bruix, and J. L. Raoul, "Treatment of intermediate-stage hepatocellular carcinoma," *Nat. Rev. Clin. Oncol.*, vol. 11, no. 9, pp. 525–535, 2014, doi: 10.1038/nrclinonc.2014.122.

[10] J. Bruix, M. Reig, and M. Sherman, "Evidence-based diagnosis, staging, and treatment of patients with hepatocellular carcinoma," *Gastroenterology*, vol. 150, no. 4, pp. 835–853, 2016.

[11] E. J. A. Morris *et al.*, "Surgical management and outcomes of colorectal cancer liver metastases," *Br. J. Surg.*, vol. 97, no. 7, pp. 1110–1118, 2010.

[12] C. E. Tatsui *et al.*, "surgery in the management of spinal metastasis," vol. 23, no. October, pp. 400–411, 2015, doi: 10.3171/2015.3.SPINE15210.Submitted.

[13] T. Livraghi, H. Mäkisalo, and P. Line, "Treatment options in hepatocellular carcinoma today Stage 0 Stage A-C," pp. 22–29, 2011, doi: 10.1177/145749691110000105.

[14] C. L. Brace, "Microwave tissue ablation: Biophysics, technology, and applications," *Crit. Rev. Biomed. Eng.*, vol. 38, no. 1, pp. 65–78, 2010, doi: 10.1615/CritRevBiomedEng.v38.i1.60.

[15] B. Imene, B. Farid, and B. Khaoula, "CT-guided microwave liver tumors ablation and automatic adjustment of frequency," vol. 2, no. 1, 2018.

[16] W. A. N'Djin *et al.*, "Capacitive micromachined ultrasound transducers for interstitial high-intensity ultrasound therapies," *IEEE Trans. Ultrason. Ferroelectr. Freq. Control*, vol. 64, no. 8, pp. 1245–1260, 2017.

[17] J. Macdonell *et al.*, "Magnetic resonance–guided interstitial high-intensity focused ultrasound for brain tumor ablation," vol. 44, no. February, pp. 1–6, 2018, doi: 10.3171/2017.11.FOCUS17613.

[18] T. R. Fosnight *et al.*, "Echo decorrelation imaging of rabbit liver and VX2 tumor during in vivo ultrasound ablation," *Ultrasound Med. Biol.*, vol. 43, no. 1, pp. 176–186, 2017.

[19] T. J. Vogl *et al.*, "Colorectal Cancer Liver Metastases: Long-Term Survival and Progression-Free Survival After Thermal Ablation Using Magnetic Resonance–Guided Laser-Induced Interstitial Thermotherapy in 594 Patients Analysis of Prognostic Factors," *Invest. Radiol.*, vol. 49, no. 1, pp. 48–56, 2014.

[20] B. M. Künzli, P. Abitabile, and C. A. Maurer, "Radiofrequency ablation of liver tumors: actual limitations and potential solutions in the future," *World J. Hepatol.*, vol. 3, no. 1, p. 8, 2011.

[21] Y. K. Cho, H. Rhim, and S. Noh, "Radiofrequency ablation versus surgical resection as primary treatment of hepatocellular carcinoma meeting the Milan criteria: a systematic review," *J. Gastroenterol. Hepatol.*, vol. 26, no. 9, pp. 1354–1360, 2011.

[22] P. Dvorak *et al.*, "Percutaneous radiofrequency and microwave ablation in the treatment of renal tumors – 10 years of experience," *Wideochirurgia I Inne Tech. Maloinwazyjne*, vol. 12, no. 4, pp. 394–402, 2017, doi: 10.5114/wiitm.2017.72322.

[23] T. Livraghi, F. Meloni, L. Solbiati, G. Zanus, and C. I. G. using A. system, "Complications of microwave ablation for liver tumors: results of a multicenter study," *Cardiovasc. Intervent. Radiol.*, vol. 35, no. 4, pp. 868–874, 2012.

[24] H. X. Xu and M. De Lu, "Technology and Method 窑 Percutaneous ultrasound - guided thermal ablation for liver tumor with artificial pleural effusion or ascites Methods : Results :

Conclusions :," vol. 29, no. 9, 2010.

[25] H. Zhi-Yu, L. Ping, Y. Xiao-Ling, C. Zhi-Gang, L. Fang-Yi, and Y. Jie, "A clinical study of thermal monitoring techniques of ultrasound-guided microwave ablation for hepatocellular carcinoma in high-risk locations," *Sci. Rep.*, vol. 7, no. December 2016, pp. 1–8, 2017, doi: 10.1038/srep41246.

[26] "Local recurrence after laparoscopic radiofrequency ablation of malignant liver tumors : Results of a contemporary series," no. January, pp. 830–834, 2017, doi: 10.1002/jso.24599.

[27] M. Huisman and M. van den Bosch, "MR-guided high-intensity focused ultrasound for noninvasive cancer treatment," *Cancer Imaging*, vol. 11, no. 1A, p. S161, 2011.

[28] K. Hynynen, "MRI-guided focused ultrasound treatments," *Ultrasonics*, vol. 50, no. 2, pp. 221–229, 2010.

[29] Y.-F. Zhou, "High intensity focused ultrasound in clinical tumor ablation," *World J. Clin. Oncol.*, vol. 2, no. 1, p. 8, 2011.

[30] A. Napoli *et al.*, "MR-guided high-intensity focused ultrasound: current status of an emerging technology," *Cardiovasc. Intervent. Radiol.*, vol. 36, no. 5, pp. 1190–1203, 2013.

[31] G. Xu *et al.*, "Follow-up of high-intensity focused ultrasound treatment for patients with hepatocellular carcinoma," *Ultrasound Med. Biol.*, vol. 37, no. 12, pp. 1993–1999, 2011.

[32] K. K. C. Ng *et al.*, "High-intensity focused ultrasound for hepatocellular carcinoma: a single-center experience," *Ann. Surg.*, vol. 253, no. 5, pp. 981–987, 2011.

[33] F. Primavesi *et al.*, "Thermographic real-time-monitoring of surgical radiofrequency and microwave ablation in a perfused porcine liver model," *Oncol. Lett.*, vol. 15, no. 3, pp. 2913–2920, 2018, doi: 10.3892/ol.2017.7634.

[34] S. Swierczynski *et al.*, "382. Thermographic monitoring of radiofrequency and microwave ablation in a perfused porcine liver model," *Eur. J. Surg. Oncol.*, vol. 40, no. 11, p. S147, 2014, doi: 10.1016/j.ejso.2014.08.372.

[35] H. Wu, L. R. Wilkins, N. P. Ziats, J. R. Haaga, and A. A. Exner, "Real-time monitoring of radiofrequency ablation and postablation assessment: Accuracy of contrast-enhanced US in experimental Rat liver model," *Radiology*, vol. 270, no. 1, pp. 107–116, 2014, doi: 10.1148/radiol.13121999.

[36] P. Wiggermann *et al.*, "Monitoring during hepatic radiofrequency ablation (RFA): Comparison of real-time ultrasound elastography (RTE) and contrast-enhanced ultrasound (CEUS): First clinical results of 25 patients," *Ultraschall der Medizin-European J. Ultrasound*, vol. 34, no. 06, pp. 590–594, 2013.

[37] Y. Z. Zhang *et al.*, "Application of high-resolution ultrasound, real-time elastography, and contrast-enhanced ultrasound in differentiating solid thyroid nodules," *Med. (United States)*, vol. 95, no. 45, 2016, doi: 10.1097/MD.0000000000005329.

[38] R. J. Dewall, T. Varghese, and C. L. Brace, "Visualizing ex vivo radiofrequency and microwave ablation zones using electrode vibration elastography," *Med. Phys.*, vol. 39, no. 11, pp. 6692–6700, 2012, doi: 10.1118/1.4758061.

[39] A. L. Abdel Gawad, Y. H. El-Sharkawy, and A. F. El-Sherif, "Classification of human teeth caries using custom non-invasive optical imaging system," *Lasers Dent. Sci.*, vol. 1, no. 2–4, pp. 73–81, 2017, doi: 10.1007/s41547-017-0008-x.

[40] T. Hennedige and S. K. Venkatesh, "Imaging of hepatocellular carcinoma: diagnosis, staging and treatment monitoring," *Cancer Imaging*, vol. 12, no. 3, p. 530, 2012.

[41] Q. Li, X. He, Y. Wang, H. Liu, D. Xu, and F. Guo, "Review of spectral imaging technology in biomedical engineering: achievements and challenges," *J. Biomed. Opt.*, vol. 18, no. 10, p. 100901, 2013.

[42] J. M. Bioucas-Dias, A. Plaza, G. Camps-Valls, P. Scheunders, N. Nasrabadi, and J. Chanussot, "Hyperspectral remote sensing data analysis and future challenges," *IEEE Geosci. Remote Sens. Mag.*, vol. 1, no. 2, pp. 6–36, 2013.

[43] H. Akbari *et al.*, "Hyperspectral imaging and quantitative analysis for prostate cancer detection," *J. Biomed. Opt.*, vol. 17, no. 7, p. 76005, 2012.

[44] L. Gao and R. T. Smith, "Optical hyperspectral imaging in microscopy and spectroscopy–a review of data acquisition," *J. Biophotonics*, vol. 8, no. 6, pp. 441–456, 2015.

[45] T. Delineation *et al.*, "An Intraoperative Visualization System Using Hyperspectral Imaging to Aid in Brain," 2018, doi: 10.3390/s18020430.

[46] H. Akbari, K. Uto, Y. Kosugi, K. Kojima, and N. Tanaka, "Cancer detection using infrared hyperspectral imaging," *Cancer Sci.*, vol. 102, no. 4, pp. 852–857, 2011, doi: 10.1111/j.1349-7006.2011.01849.x.

[47] Y. H. El-Sharkawy, "Optical Properties of Non-Malignant and Malignant Breast Tissue Determined by Surface Displacement of Laser-Induced Photoacoustic Generation," *Int. J. Opt. Photonic Eng.*, vol. 1, no. 1, pp. 1–8, 2016, doi: 10.35840/2631-5092/4502.

[48] D. M. Schuster, P. T. Nieh, and G. Z. Chen, "Hyperspectral imaging and quantitative analysis for prostate cancer detection," no. May, 2020, doi: 10.1117/1.JBO.17.7.076005.

[49] P. C. Benias and D. L. Carr-Locke, "Principles of Electrosurgery," *Ercp*, pp. 86-92.e1, 2019, doi: 10.1016/b978-0-323-48109-0.00011-0.

[50] T. Adão *et al.*, "Hyperspectral imaging: A review on UAV-based sensors, data processing and applications for agriculture and forestry," *Remote Sens.*, vol. 9, no. 11, 2017, doi: 10.3390/rs9111110.

[51] S. S. M. Noor, K. Michael, S. Marshall, and J. Ren, "Hyperspectral image enhancement and mixture deep-learning classification of corneal epithelium injuries," *Sensors (Switzerland)*, vol. 17, no. 11, 2017, doi: 10.3390/s17112644.

[52] M. Halicek, H. Fabelo, S. Ortega, G. M. Callico, and B. Fei, "In-vivo and ex-vivo tissue analysis through hyperspectral imaging techniques: Revealing the invisible features of cancer," *Cancers (Basel).*, vol. 11, no. 6, pp. 1–30, 2019, doi: 10.3390/cancers11060756.

[53] K. Muhammad, J. Ahmad, H. Farman, and M. Zubair, "A Novel Image Steganographic Approach for Hiding Text in Color Images using HSI Color Model," p. 11, 2015, doi: 10.5829/idosi.mejsr.2014.22.05.21946.

[54] V. Kumar and P. Gupta, "Importance of Statistical Measures in Digital Image Processing," *Int. J. Emerg. Technol. Adv. Eng.*, vol. 2, no. 8, pp. 56–62, 2012.

**Mohamed Hisham Aref** is PhD Candidate at Military Technical College, Biomedical Engineering department. He received his BS degree in Biomedical Engineering from Military Technical College in 2006 and his MS degree from Cairo University, Faculty of engineering in 2012, respectively, He is highly skilled & talented biomedical engineer with more than 14 years of practical experience in the design & improvement of the medical equipment's disease diagnosis, treatments & preventions. His current PhD topic in "Monitoring & Control of Tumor Thermal Ablation using Advanced Ultrasound Imaging Technologies. His current research interests include Thermal Ablation, US imaging technologies, Cancer Early detection, Medical Gases Design, Hyperbaric Oxygen Therapy. He is a member of IEEE.



**Ibrahim H. Aboughaleb** is PhD Candidate at Military Technical College, Biomedical Engineering department. He received his BS degree in Biomedical Engineering from Military Technical College in 2006 and his MS degree from Cairo University, Faculty of engineering in 2014, respectively, Strong research professional and Experienced Biomedical Engineer with a demonstrated history of working in the hospital & health care industry. Skilled in Medical Devices, Biomedical Electronics, Management, Circuit Analysis, and Biomedical Engineering.



**Dr. Mohamed Rabie**, received the Master's degree in Biomedical engineering from the University Of Dundee, United Kingdom in September 2013 and the Ph.D. degree in Biomedical Engineering from University of Strathclyde, United Kingdom, in 2018. He is currently a lecturer in Biomedical Engineering Department at the Military Technical College, Cairo, Egypt. He is engaged in research on Clinical Engineering, Robotic Systems, Imaging Processing and Endoscopy.

**Prof.\ Yasser H. El-Sharkawy** is professor and Head of Biomedical Engineering department at Military Technical College. He received his BS and MS degrees in physics from the University of Optics in 1993 and 1996, respectively, and his PhD degree in optics from the Institute of Laser and Technology in 2006. He is the author of more than 54 journal papers. His current research interests include photo acoustic imaging used for breast cancer detection, Biophysics and Medical Physics, Medical Imaging and analysis, Biomedical Engineering.

To Submit Your Article Click Here: **Submit Manuscript**

**Ready to submit your research? Choose Auctores and benefit from:**

- ❖ fast, convenient online submission
- ❖ rigorous peer review by experienced research in your field
- ❖ rapid publication on acceptance
- ❖ authors retain copyrights
- ❖ unique DOI for all articles
- ❖ immediate, unrestricted online access

At Auctores, research is always in progress.

Learn more www.auctoresonline.org/journals/biomedical-research-and-clinical-reviews-